HHS Public Access

Author manuscript

Hepatology. Author manuscript; available in PMC 2021 May 27.

Published in final edited form as:

Hepatology. 2017 August ; 66(2): 498–509. doi:10.1002/hep.29199.

Hepatic FXR/SHP Axis Modulates Systemic Glucose and Fatty Acid Homeostasis in Aged Mice

Kang Ho Kim[1], **Sungwoo Choi**[2], **Ying Zhou**[1,3], **Eun Young Kim**[4], **Jae Man Lee**[4], **Pradip K. Saha**[1], **Sayeepriyadarshini Anakk**[5], **David D. Moore**[1,2,3]

[1]Department of Molecular and Cellular Biology, Baylor College of Medicine, Houston, TX

[2]Program in Developmental Biology, Baylor College of Medicine, Houston, TX

[3]Integrative Molecular and Biomedical Sciences Graduate Program, Baylor College of Medicine, Houston, TX

[4]Department of Biochemistry and Cell Biology, School of Medicine, Kyungpook National University, Daegu, Republic of Korea

[5]Department of Molecular and Integrative Physiology, University of Illinois at Urbana-Champaign, Urbana, IL

Abstract

The nuclear receptors farnesoid X receptor (FXR; NR1H4) and small heterodimer partner (SHP; NR0B2) play crucial roles in bile acid homeostasis. Global double knockout of FXR and SHP signaling (DKO) causes severe cholestasis and liver injury at early ages. Here, we report an unexpected beneficial impact on glucose and fatty acid metabolism in aged DKO mice, which show suppressed body weight gain and adiposity when maintained on normal chow. This phenotype was not observed in single *Fxr* or *Shp* knockouts. Liver-specific *Fxr/Shp* double knockout mice fully phenocopied the DKO mice, with lower hepatic triglyceride accumulation, improved glucose/insulin tolerance, and accelerated fatty acid use. In both DKO and liver-specific *Fxr/Shp* double knockout livers, these metabolic phenotypes were associated with altered expression of fatty acid metabolism and autophagy-machinery genes. Loss of the hepatic FXR/SHP axis reprogrammed white and brown adipose tissue gene expression to boost fatty acid usage.

Conclusion: Combined deletion of the hepatic FXR/SHP axis improves glucose/fatty acid homeostasis in aged mice, reversing the aging phenotype of body weight gain, increased adiposity, and glucose/insulin tolerance, suggesting a central role of this axis in whole-body energy homeostasis.

ADDRESS CORRESPONDENCE AND REPRINT REQUESTS TO: David D. Moore, Ph.D., Department of Molecular and Cellular Biology, Baylor College of Medicine, One Baylor Plaza, Houston, Texas 77030, moore@bcm.edu.
Author names in bold designate shared co-first authorship.

Potential conflict of interest: Nothing to report.

Supporting Information

Additional Supporting Information may be found at onlinelibrary.wiley.com/doi/10.1002/hep.29199/suppinfo

Hepatic metabolic pathways are tightly controlled by diverse transcriptional programs, including those directed by a number of nuclear receptors. Among them, constitutive androstane receptor, pregnane X receptor, hepatocyte nuclear factor 4 alpha, farnesoid X receptor (FXR), and small heterodimer partner (SHP) selectively expressed in liver and have pivotal functions in metabolic pathways such as bile acid homeostasis, fatty acid and glucose metabolism, and xenobiotic detoxification.[1] Loss of these functions causes serious liver diseases like cholestasis, hepatic inflammation, fibrosis, cirrhosis, and hepatocellular carcinoma.

FXR and SHP have been implicated in bile acid homeostasis. FXR was first identified as an orphan nuclear receptor, but bile acids like chenodeoxycholic acid were identified as endogenous agonist ligands.[2] Activation of FXR directly activates target genes in bile acid metabolism, including the *Bsep*, and inhibits others, particularly cytochrome P450, family 7, subfamily a, polypeptide 1 (*Cyp7a1*), with the overall effect of facilitating enterohepatic bile acid circulation, restraining bile acid synthesis, and maintaining homeostasis.[2] SHP is both a transcriptional repressor and a direct FXR target. It interacts with a variety of other nuclear receptors such as hepatocyte nuclear factor 4 alpha, liver receptor homolog-1, and peroxisome proliferator–activated receptors and blocks their transactivation.[3] Thus, SHP induction by FXR suppresses Cyp7a1 expression by inhibiting liver receptor homolog-1 and hepatocyte nuclear factor 4 alpha–mediated transcription, resulting in the suppression of *de novo* bile acid synthesis.[2]

In this linear model of FXR/SHP regulation of bile acid homeostasis, loss of FXR should be epistatic to SHP and the phenotypes of *Fxr* single knockouts and *Fxr/Shp* double knockouts (DKO) should be quite similar. However, in contrast to the relatively modest dysregulation of bile acid homeostasis observed in the single knockouts, DKO mice develop juvenile-onset cholestasis with enlarged liver size and severe liver damage as early as 3 weeks of age. This is also associated with a much greater increase of *Cyp7a1* expression in DKO mice compared to single knockouts.[4] This indicates that FXR and SHP have both overlapping and nonoverlapping functions in bile acid homeostasis, with complete disruption of the FXR/SHP axis leading to severe liver damage due to uncontrolled bile acid overload.

In addition to bile acid metabolism, both FXR and SHP have been reported to regulate glucose and fatty acid homeostasis. Under normal conditions, *Fxr* knockout mice show high serum triglyceride and free fatty acid levels, which are also associated with impaired glucose tolerance and insulin resistance.[5–7] Mixed results have been observed in *Shp* knockout mice with different backgrounds, but congenic C57BL/6 *Shp* knockout mice show increased β-oxidation without changes in glucose/insulin tolerance.[8,9]

Here we explored basal metabolic changes in response to complete disruption of the FXR/SHP axis. Normal chow-fed DKO mice unexpectedly show significantly decreased body weight and white adipose tissue (WAT) mass at 4-5 months of age, which is maintained until 1 year of age. In contrast to *Fxr* single knockout mice, aged DKO mice show greatly improved glucose and fatty acid homeostasis. Interestingly, these phenotypes are completely reproduced in mice with liver-specific *Fxr/Shp* deletion (FS^{LKO}). These

unique phenotypes identify a central role for the hepatic FXR/SHP axis in the control of whole-body energy metabolism.

Materials and Methods

ANIMAL STUDIES

Male mice were used for all experiments. C57BL/6J wild-type (WT) and Alb-Cre/+ mice were obtained from the Jackson Laboratory (000664 and 003574). DKO mice have been described.[4] *Fxr*$^{F/F}$ and *Shp*$^{F/F}$ mice were kindly provided by Dr. Johan Auwerx (Ecole Polytechnique Federale de Lausanne, Switzerland). Alb-cre/+, *Fxr*$^{F/F}$, and *Shp*$^{F/F}$ mice were crossed to generate an Alb-cre/+;*Fxr*$^{F/F}$;*Shp*$^{F/F}$ founder. Alb-cre/+; *Fxr*$^{F/F}$;*Shp*$^{F/F}$ mice exhibited a possibility of incomplete deletion of *Fxr* and *Shp* floxed alleles (7.4% of *Fxr* and 0.5% of *Shp* expression were still detected compared to *Fxr*$^{F/F}$;*Shp*$^{F/F}$ mice) at younger age (data not shown). To minimize inefficient deletion of multiple flox alleles by the Alb-cre transgene,[10–12] Alb-Cre/+;*Fxr*$^{F/F}$;*Shp*$^{F/F}$ mice were further crossed with DKO (*Fxr*$^{-/-}$;*Shp*$^{-/-}$) mice to generate Alb-Cre/+;*Fxr*$^{F/-}$;*Shp*$^{F/-}$ (FS^{LKO}) or control littermates (*Fxr*$^{F/-}$;*Shp*$^{F/-}$, FS^{Cont}) carrying only single copies of the two floxed alleles. FS^{LKO} mice had only 2.7% of *Fxr* and 0.05% of *Shp* expression compared to FS^{Cont} mice (data not shown). Glucose tolerance tests were carried out by intraperitoneal injection of glucose (2 g/kg body weight) after 24-hour fasting. Insulin tolerance tests were performed by intraperitoneal injection of low-dose insulin (0.5 U/kg body weight). Blood glucose levels were measured by tail bleeds at indicated time points after glucose or insulin injection. For FXR activation, GW4064 (100 mg/kg, oral gavage) was administered twice a day (first injection at midnight and second injection at noon, then sacrificed at 6:00 PM). All animal studies and procedures were approved by the Institutional Animal Care and Use Committee of the Baylor College of Medicine.

DETERMINATION OF INSULIN, TRIGLYCERIDE, AND TOTAL BILE ACID LEVELS

Serum was separated from whole blood using a gel barrier collection tube (3T-MGA, CAPIJECT). Liver extracts were prepared by either a 1:2 chloroform:methanol mixture (for triglycerides, modified Folch method) or 75% ethanol (for total bile acids). Each sample was analyzed to determine the triglyceride level (Infinity Triglycerides Reagent, TR22421; Thermo Fisher Scientific) and the total bile acid level (Total Bile Acids Assay, GWB-BQK090; GENWAY Biotech). The serum insulin level was measured by the Rat/Mouse Insulin ELISA kit (EZRMI-13K; EMD Millipore).

MOUSE PHENOTYPING

Body composition (fat mass and lean mass) was observed by EchoMRI (EchoMRI LLC). The Oxymax-Comprehensive Laboratory Animal monitoring system (Columbus Instruments) was used to measure VO_2 and VCO_2 at the Baylor College of Medicine Mouse Metabolism Core. All parameters were monitored every 24 minutes for 24 hours and normalized to lean mass (n = 3 per group). Respiratory exchange ratio (RER) was calculated as follows: $RER = VCO_2/VO_2$.

HISTOLOGY

For oil-red O staining, optimal cutting temperature–embedded frozen tissue was sectioned at 5-7 μm and fixed in 10% neutral buffered formalin (BDH0502; BDH Chemicals). After washing with distilled water, dried slides were subsequently incubated with 100% propylene glycol and 0.5% oil-red O solution (O-1516; Sigma). Stained slides were washed with 85% propylene glycol solution and distilled water, then mounted with glycerin. For hematoxylin and eosin, paraffin-embedded liver and adipose tissues were used. Adipocyte or lipid droplet size from 7 or 8 nonoverlapped images per each mouse was quantified with the ADIPOSOFT program, which is an open-source software by the Imaging Unit of the Center for Applied Medical Research at the University of Navarra (available at http://imagej.net/Adiposoft).

ANALYSIS OF THE GENE EXPRESSION OMNIBUS DATA SET (MICROARRAY AND CHROMATIN IMMUNOPRECIPITATION SEQUENCING)

The GSE20599 data set was used for DKO gene expression profile. The 5-week-old WT control (GSM 517341 and GSM517342) and DKO (GSM517347 and GSM513748) mice were analyzed with the GEO2R web-based program. The Illumina ID numbers showing a significant difference ($P < 0.01$) were further analyzed by DAVID Bioinformatics Resources 6.7 Tools (https://david.ncifcrf.gov). Representative groups in each category (Gene Ontology-Biological Pathway, Gene Ontology-Cellular Component, and Kyoto Encyclopedia of Genes and Genomes Pathway) are shown in Supporting Fig. S5. Direct fatty acid metabolism genes involved in fatty acid synthesis, desaturation, and elongation were separately analyzed and visualized by Gene Cluster 3.0 (http://bonsai.hgc.jp/~mdehoon/software/cluster/) and Java Treeview program (http://jtreeview.sourceforge.net/). For chromatin immunoprecipitation (ChIP) sequencing (seq) results, FXR (University of California Santa Cruz Genome Browser Custom Tracks, https://genome.ucsc.edu/goldenPath/customTracks/custTracks.html) and SHP (GSE74913,[13] Gene Expression Omnibus data set) binding were visualized using Integrative Genomics Viewer software (Broad Institute).

REAL-TIME QUANTITATIVE PCR

Total RNA was isolated by TRIzol reagent (15596; Thermo Fisher Scientific) and converted into complementary DNA by the qScript Reverse Transcriptase Kit (95047; Quanta Bio). The gene expression level was quantified by quantitative PCR using the Light-Cycler 480 Real-Time PCR System (Roche) with KAPA SYBR FAST qPCR Kits (KAPA Biosystems). mRNA amounts were calculated by the comparative cycle threshold method (ΔΔCt method) with normalization to glyceraldehyde-3-phosphate dehydrogenase mRNA. Primer information is listed in Supporting Table S1.

ChIP-PCR ANALYSIS

Details of the ChIP-PCR assay have been described.[14] Briefly, 100 mg of each liver tissue was crosslinked by 1% formaldehyde solution and homogenized using a Dounce homogenizer. Isolated nuclei were further sonicated with a Bioruptor sonicator (Diagenode) and immunoprecipitated with anti-FXR and SHP antibody (sc-13063x and sc-30169,

respectively; Santa Cruz Biotechnology). Precipitated DNA was analyzed by quantitative PCR using *Atg7* and *Atg12* ChIP-PCR primers as listed in Supporting Table S2.

STATISTICAL ANALYSIS

All results are presented as mean ±standard error of the mean, and *P* values between two groups were calculated by two-tailed Student *t* test (**P*< 0.05, ***P*< 0.01, ****P*< 0.005). Comparison of three or more groups was analyzed by one-way analysis of variance (ANOVA). Statistical significance of the ANOVA was determined by a *post hoc t* test with Bonferroni correction. With a family of six comparisons (four groups), an original significance was corrected into $^{\#}P$< 0.0083 (=0.05/6), $^{\#\#}P$< 0.0017 (=0.01/6), and $^{\#\#\#}P$< 0.00083 (=0.005/6).

Results

HEPATIC FXR/SHP SIGNALING CONTROLS FAT MASS AND HEPATIC LIPID ACCUMULATION

Combined deletion of *Fxr* and *Shp* (DKO) strongly impacts bile acid metabolism from an early age, with markedly elevated bile acid levels associated with hepatomegaly and eventually liver cancer in aged DKO mice.[4,15] In addition, chow-fed DKO mice show decreased body weight gain after 4-5 months and maintain lower body weight until at least 1 year of age (Fig. 1A,C). In accord with previous reports,[16–18] aged WT mice exhibit increased adipose tissue and fatty liver relative to younger mice (Fig. 1B). Both body weight and fat tissue mass were dramatically reduced in DKO mice (Fig. 1B,C). Importantly, this was not associated with overall growth retardation (Fig. 1D). This metabolic phenotype was not observed in *Fxr* or *Shp* single knockouts (Supporting Fig. S1), indicating coordinate action of the FXR/SHP axis.

Both *Fxr* and *Shp* are expressed in multiple organs outside the liver, including intestine and kidney. To address whether the hepatic FXR/SHP axis plays a major role in this phenotype, we generated liver-specific *Fxr/Shp* double knockout (FS^{LKO}) mice. To minimize inefficient deletion of multiple floxed alleles[10–12] and simplify the generation and analysis of mutant mice and littermate controls, FS^{LKO} mice were heterozygous for floxed and knockout alleles (*Alb-Cre;*$Fxr^{F/-}$;$Shp^{F/-}$) and compared to FS^{Cont} littermates lacking the Cre transgene ($Fxr^{F/-}$;$Shp^{F/-}$). FS^{Cont} mice did not differ from fully WT mice with regard to body weight or other basic phenotypes.

Like DKO mice, aged FS^{LKO} mice had substantially lower body weight compared to control littermates (FS^{Cont}) (Fig. 2A,B), without any body length difference (Fig. 2C). Notably, body fat mass was strongly decreased in FS^{LKO} (Fig. 2D). In contrast to the pale color of FS^{Cont} liver, FS^{LKO} liver had a dark color with less hepatic lipid accumulation (Fig. 2E,F), which is somewhat opposite to a previous report.[7] However, serum triglyceride levels remained high in both DKO and FS^{LKO} mice (Fig. 2F), suggesting altered fatty acid metabolism in liver. Total bile acid levels were elevated to a similar extent in DKO and FS^{LKO} mice (Fig. 2F). Overall, disruption of the hepatic FXR/SHP axis limits aging-induced body weight gain and lowers lipid accumulation in liver.

FS^{LKO} IMPROVES GLUCOSE HOMEOSTASIS IN AGED MICE

Excess hepatic lipid accumulation is a hallmark of metabolic disease.[19] With phenotypic changes including weight gain and body fat accumulation, aged mice develop glucose intolerance and insulin resistance.[17] We next examined whether the phenotypic changes in aged DKO and FS^{LKO} mice are accompanied by improved glucose homeostasis. Blood glucose levels did not differ in control and FS^{LKO} mice in the fed state, but fasting glucose was significantly decreased in FS^{LKO} mice (Fig. 3A). Serum insulin was significantly lower both in the fed and in the fasted status (Fig. 3B), resulting in a dramatic decrease of the homeostasis model assessment of insulin resistance index in FS^{LKO} mice (Fig. 3C). Consistent with this, both glucose tolerance and insulin tolerance tests revealed improved insulin sensitivity in aged FS^{LKO} mice (Fig. 3D,E). In accord with their decreased body weight, DKO mice also showed lower insulin level and homeostasis model assessment of insulin resistance index with improved insulin responsiveness (Supporting Fig. S2).

FS^{LKO} EXCLUSIVELY USES FATTY ACIDS AS PRIMARY SUBSTRATES IN OXIDATIVE METABOLISM

To assess energy balance in FS^{LKO} mice, we used indirect calorimetry analysis. Despite their decreased body weight gain and fat composition, basal food intake and oxygen consumption rate (VO_2) were not different in FS^{LKO} mice and controls (Supporting Fig. S3; Fig. 4A). However, carbon dioxide production (VCO_2) was significantly decreased, particularly during the daytime, and RER was also markedly reduced in both day and night (Figs. 4B,C), demonstrating increased fat usage. The difference between FS^{Cont} and FS^{LKO} mice was maximal during the feeding to fasting transition (5:00 AM-1:00 PM), indicating a rapid induction of fat usage in the early fasting state.

THE FXR/SHP AXIS ALTERS HEPATIC FATTY ACID METABOLISM

To investigate the mechanism of the impact of the hepatic FXR/SHP axis on fatty acid usage, we screened hepatic gene expression in aged FS^{LKO} mice. In contrast to our expectation, mRNA expression of most genes involved in fatty acid synthesis, fatty acid uptake, lipolysis, fatty acid oxidation, and glucose metabolism was not changed (Supporting Fig. S4). We interrogated gene expression in younger DKO mice by microarray (Gene Expression Omnibus Data set, GSE20599) to identify novel candidate genes and functional groups regulated by the FXR/SHP axis and performed gene ontology/Kyoto Encyclopedia of Genes and Genomes pathway analysis using DAVID tools (National Institute of Allergy and Infectious Diseases; $P < 0.01$). Gene ontology analysis of biological pathways and cellular components indicated altered expression of fatty acid metabolism and autophagy/lysosomal genes (Supporting Fig. S5A,B). Kyoto Encyclopedia of Genes and Genomes pathway analysis also indicated that multiple genes in fatty acid metabolism and lysosomal pathways were significantly affected (Supporting Fig. S5C).

Although direct fatty acid/triglyceride synthesis genes were not affected by FXR/SHP axis deletion (Supporting Fig. S4), many enzymes involved in fatty acid elongation and the desaturation process were changed (Fig. 5A). Several genes identified by the microarray result from young mice were not altered in the older livers but others such as *Scd2, Acsl4, Elovl2, Acsl1*, and *Elovl3* were consistently regulated in aged DKO and FS^{LKO} mice (Fig.

5C,D). Interestingly, although none of these genes behaved in the same manner, loss of the FXR/SHP axis had a profound effect on *Scd2* and *Elovl3* expression (Fig. 5E). Expression of *Elovl3*, which is involved in saturated or monounsaturated fatty acid elongation, was primarily dependent on FXR (decreased by 79.5% in *Fxr* knockout relative to WT) but not on SHP (Fig. 5E). However, it was particularly strongly blunted in DKO (97.0%; Fig. 5E) and FS^{LKO} (94.1%; Fig. 5D) mice. Its expression was significantly enhanced by FXR agonist treatment (Fig. 5F), suggesting it as a novel target of the hepatic FXR/SHP axis in hepatic fatty acid metabolism.

HEPATIC FXR/SHP AXIS REGULATES AUTOPHAGY GENE EXPRESSION

Autophagy is a cellular catabolic process that degrades and recycles long-lived proteins and cytoplasmic organelles. Defective hepatic autophagy imposes impaired insulin and glucose homeostasis in obesity, whereas adenoviral ATG7 restoration reverses it.[20] Previously, we showed that FXR activation suppresses hepatic autophagy, whereas *Fxr* knockout enhanced autophagic vesicle formation.[14]

In DKO and FS^{LKO} mice, many genes encoding components of the autophagy machinery, including *Atg7* and *Atg12*, were significantly increased (Fig. 6A; Supporting Fig. S5A), but they were not changed in *Fxr* or *Shp* single knockouts (Fig. 6B). ChIP-seq analysis (GSE74913 and Custom Annotation Tracks at the University of California Santa Cruz genome browser) also found many FXR and SHP binding sites in *Atg7* and *Atg12* regulatory regions (Fig. 6C), which were confirmed by ChIP-PCR analysis (Fig. 6D). Together, these data indicate that loss of the hepatic FXR/SHP axis induces autophagy gene expression, leading to the restoration of autophagic flux in liver.

LOSS OF HEPATIC FXR/SHP ALTERS FATTY ACID METABOLISM IN ADIPOSE TISSUE

Although it only directly affects the liver, FS^{LKO} affects whole-body phenotypes including aging-induced weight gain and alterations of glucose/fatty acid metabolism (Fig. 2D), improved peripheral insulin sensitivity (Fig. 3E), and preferred fatty acid usage (Fig. 4C). Thus, we investigated the impact of deletion of the hepatic FXR/SHP axis in other adipose tissue, which is the most affected (Figs. 1B and 2A). Direct histological analysis of three different adipose depots (epididymal WAT [eWAT], inguinal WAT [iWAT], brown adipose tissue [BAT]) showed significant decrease of aging-induced adipocyte hypertrophy (Fig. 7A), characterized by lower adipocyte volume (eWAT and iWAT) or lipid droplet size (BAT) (Fig. 7A,B). Gene expression profiling also revealed that many genes of lipolysis, β-oxidation, and thermogenesis were up-regulated (Fig. 7C). This indication of enhanced fatty acid use in FS^{LKO} adipose tissue suggests crosstalk between liver and adipose tissue.

One potential mechanism for such crosstalk is increased expression of hepatic fibroblast growth factor 21 (FGF-21) and intestinal FGF-15, which are target genes of FXR and share antiobesity and antidiabetic effects in common.[21] In young and old DKO mice, *Fgf21* mRNA was increased relative to WT mice (Supporting Fig. S6A). Similar results were observed in younger FS^{LKO} livers relative to FS^{Cont} livers, but in the older mice *Fgf21* gene expression was elevated to a comparable extent in both FS^{Cont} and FS^{LKO} livers relative to fully WT livers (Supporting Fig. S6B). In contrast, *Fgf15* expression was strongly

diminished in DKO ileum and unchanged in FS^{LKO} ileum (Supporting Fig. S6C,D), suggesting that FGF-15 is not a main mediator of these phenotypes.

Discussion

Aging is a major contributor to the metabolic syndrome that links obesity, insulin resistance, peripheral lipid accumulation, and chronic inflammation.[22] As aging progresses, chronic imbalance of energy intake and expenditure results in spillover of excess nutrients into liver and skeletal muscle, promoting hepatic steatosis and muscle insulin resistance.[23] Many studies have shown increased body weight, especially fat mass, and decreased physical activity, resulting in glucose intolerance and insulin resistance in aging mice.[17,24]

We found that cholestatic DKO mice unexpectedly show an antiobesity phenotype. The difference in body weight begins at approximately 12 weeks and becomes much more apparent at later ages. At the later stages, their liver pathology is unexpectedly improved relative to WT controls. This age-related phenotype is unexpected from previous observations that young DKO mice display hepatic microsteatosis, elevated hepatic triglyceride accumulation, and focal inflammation due to cholestatic liver injury[4] and that decreased FXR expression is associated with elevated triglyceride accumulation and endoplasmic reticulum stress in 18-month-old WT mice.[25] The lack of any impact on growth, as indicated by body length, suggests that the decreased body weight is not secondary to liver failure or another pathology. In accord with this, and the improved liver pathology, aged DKO mice show beneficial effects on glucose and fatty acid metabolism compared to age-matched WT (Fig. 1; Supporting Fig. S2). These DKO phenotypes are also observed in FS^{LKO} mice (Fig. 2), suggesting an exclusive role of the hepatic FXR/SHP axis in glucose and fatty acid metabolism of aged mice. At the molecular level, we suggest that these phenotypes are a reflection of changes in both hepatic gene expression (Figs. 5 and 6) and crosstalk with adipose tissues (Fig. 7). Overall, these results collectively explain how deletion of the hepatic FXR/SHP axis coordinates whole-body glucose and fatty acid metabolism in aged mice.

Both DKO and FS^{LKO} mice exhibit cholestatic liver injury from an early age and spontaneous hepatic tumorigenesis much later. The liver cancer phenotype can be observed as early as 9 months old and spreads through the liver at 15-17 months age.[15] This suggests that the decreased body weight in older DKO mice could be a consequence of cancer-associated illness. However, the antiobesity effect of FXR/SHP loss was evident from a young age (~12 weeks; Fig. 1A) when DKO mice are free from liver cancer.

Furthermore, aged DKO and FS^{LKO} unexpectedly showed decreased cholestatic liver injury (alanine aminotransferase/aspartate aminotransferase levels 600-800 U/L in young DKO versus 200-300 U/L in old DKO)[4] (Supporting Fig. S7), and they are relatively healthy without signs of severe illness. These results suggest a direct role of the FXR/SHP axis in whole-body energy homeostasis.

Previously, mixed results have been reported for the impact of FXR or SHP on obesity and glucose homeostasis in various models such as high-fat diet–fed mice or *leptin*-deficient

(*ob/ob*) mice.[5,6,8,9,26–29] In our results, *Fxr* and *Shp* single knockouts exhibited marginal effects regardless of their age (Supporting Fig. S1), whereas aged DKO and FS^{LKO} mice had profound effects on body weight gain and adiposity (Figs. (1 and 2); Supporting Fig. S1). Gene expression profiling also supports the cooperative role of the hepatic FXR/SHP axis (Figs. 5 and 6), implying that the hepatic FXR/SHP axis has distinct roles to coordinate hepatic metabolism and to amplify their impacts on whole-body energy homeostasis in aged mice.

Primary screening of hepatic metabolic gene expression did not uncover an obvious mechanism for the antisteatotic phenotype of FS^{LKO} liver because most fatty acid synthesis, uptake, and breakdown genes are unchanged (Supporting Fig. S4). However, we identified *Elovl3* as a novel target gene of the FXR/SHP axis, with *Elovl3* mRNA almost completely lost in DKO and FS^{LKO} livers. This gene encodes a hepatic microsomal enzyme involved in the production of saturated or monosaturated very long-chain fatty acids (C20-C22), which are important constituents of triglyceride synthesis.[30,31] Global ablation of *Elovl3* restricts body weight gain, adipose tissue expansion, and hepatic lipid accumulation.[30] The timing of the onset of the weight phenotype and the initial magnitude is similar to that in DKO mice, although *Elovl3* knockouts gain more weight at later ages. In contrast to the DKO and FS^{LKO} livers, *Elovl3* knockouts showed modest but significant decreases in lipogenic gene expression.[30] Multiple transcription factors including several nuclear receptors have been reported to regulate *Elovl3* gene expression in various tissues [32–34] *Elovl3* expression is strongly decreased in the *Fxr* knockout and, in contrast to the expected role of SHP as a repressor, further decreased rather than increased in both DKO and FS^{LKO} livers (Fig. 5D–F). ChIP-seq data confirm the recruitment of FXR and SHP near *Elovl3* gene loci (data not shown). These results suggest an unexpectedly important role for the regulation of *Elovl3* expression by the FXR/SHP axis.

Another potentially relevant target of hepatic gene expression is increased autophagy (Fig. 6). With aging, diminished autophagic activity contributes to many age-related complications.[35] Hepatic autophagy is involved in the breakdown of stored lipid, and its inhibition promotes the initial development of hepatic steatosis and liver injury.[36] On the contrary, antiaging calorie restriction ameliorates hepatic autophagy functions as well as many metabolic parameters.[37] Also, direct restoration of autophagic flux conserves hepatic function and improves whole-body glucose homeostasis.[20,38] Many autophagy-related genes are induced in FS^{LKO} livers, and increased autophagy may contribute to the inhibition of hepatic lipid accumulation and improved glucose homeostasis.

The ability of the FS^{LKO} to recapitulate whole-body DKO phenotypes is not just a consequence of metabolic changes in the liver. Notably, disruption of the hepatic FXR/SHP axis influences WAT and BAT gene expression to facilitate fat usage (Fig. 7A–C). Two distinct mechanisms may account for how FS^{LKO} affects adiposity and β-oxidation in peripheral tissues. The most direct is the activation of Takeda G protein–coupled bile acid receptor 5 in BAT by high serum bile acid levels in FS^{LKO} (Fig. 2F). Takeda G protein–coupled bile acid receptor 5 is a bile acid-sensing G protein–coupled receptor that is highly expressed in metabolically active tissues, including adipose. Bile acid supplementation or direct Takeda G protein–coupled bile acid receptor 5 agonist treatment leads to weight loss,

improved glucose metabolism, enhanced energy expenditure, and increased fat usage through the induction of cyclic adenosine monophosphate levels and *Dio2* expression in BAT,[39–41] which is similar to what is observed in DKO and FS^{LKO} (Fig. 7C; Supporting Fig. S8). This may be reinforced by the secretion of the hepatokine FGF-21. FGF-21 is a stress-induced hormone that has many beneficial effects on glucose and fatty acid homeostasis in various metabolic tissues.[42] FGF-21 is known to be regulated by peroxisome proliferator–activated receptor alpha and other transcription factors,[43–45] and FXR and SHP have been shown to suppress peroxisome proliferator–activated receptor alpha activity.[8,14] We found that *Fgf21* expression is significantly up-regulated in DKO mice regardless of their age, indicating a possibility of an FGF-21-mediated effect on obesity and insulin resistance in aged DKO mice. Although FGF-21 was also elevated in young and old FS^{LKO} livers relative to WT mice, it was not different between FS^{LKO} and FS^{Cont} livers (Supporting Fig. S6), indicating that it does not contribute to the substantial differences between their body weights and metabolic profiles.

Collectively, we conclude that combined deletion of the FXR/SHP axis has dramatic effects on whole-body energy homeostasis in aged mice. Like DKO, FS^{LKO} also suppresses weight gain and improves glucose/insulin sensitivity, suggesting a central role of hepatic FXR/SHP axis. In liver, these beneficial effects in FS^{LKO} may be accounted for by altered expression of fatty acid metabolism and autophagy genes. In addition, FS^{LKO} liver communicates with WAT and BAT to enhance fatty acid usage and to decrease peripheral adiposity, implicating tissue-to-tissue crosstalk in whole-body energy homeostasis in aged mice.

Supplementary Material

Refer to Web version on PubMed Central for supplementary material.

Acknowledgment:

We thank Johan Auwerx (École Polytechnique Fédérale de Lausanne in Switzerland) for $Fxr^{F/F}$, $Shp^{F/F}$ mice and Jongsook Kim Kemper (University of Illinois at Urbana-Champaign) for technical advice on the SHP ChIP assay and Mouse Metabolism Core under Advanced Technology Cores in Baylor College of Medicine for technical supports.

Supported by the National Institutes of Health (U19 DK062434).

Abbreviations:

ANOVA	analysis of variance
BAT	brown adipose tissue
ChIP	chromatin immunoprecipitation
ChIP-seq	ChIP sequencing
Cyp7a1	cytochrome P450, family 7, subfamily a, polypeptide 1
DKO	Fxr and Shp double knockout
eWAT	epididymal WAT

FGF	fibroblast growth factor
FS^{Cont}	control littermate
FS^{LKO}	Fxr and Shp liver-specific knockout
FXR	farnesoid X receptor
iWAT	inguinal WAT
RER	respiratory exchange ratio
SHP	small heterodimer partner
WAT	white adipose tissue
WT	wild type

REFERENCES

1). Fuchs CD, Traussnigg SA, Trauner M. Nuclear receptor modulation for the treatment of nonalcoholic fatty liver disease. Semin Liver Dis 2016;36:69–86. [PubMed: 26870934]

2). Modica S, Gadaleta RM, Moschetta A. Deciphering the nuclear bile acid receptor FXR paradigm. Nucl Recept Signal 2010;8:e005. [PubMed: 21383957]

3). Zhang Y, Hagedorn CH, Wang L. Role of nuclear receptor SHP in metabolism and cancer. Biochim Biophys Acta 2011; 1812:893–908. [PubMed: 20970497]

4). Anakk S, Watanabe M, Ochsner SA, McKenna NJ, Finegold MJ, Moore DD. Combined deletion of Fxr and Shp in mice induces Cyp17a1 and results in juvenile onset cholestasis. J Clin Invest 2011;121:86–95. [PubMed: 21123943]

5). Cariou B, van Harmelen K, Duran-Sandoval D, van Dijk TH, Grefhorst A, Abdelkarim M, et al. The farnesoid X receptor modulates adiposity and peripheral insulin sensitivity in mice. J Biol Chem 2006;281:11039–11049. [PubMed: 16446356]

6). Ma K, Saha PK, Chan L, Moore DD. Farnesoid X receptor is essential for normal glucose homeostasis. J Clin Invest 2006;116: 1102–1109. [PubMed: 16557297]

7). Sinal CJ, Tohkin M, Miyata M, Ward JM, Lambert G, Gonzalez FJ. Targeted disruption of the nuclear receptor FXR/BAR impairs bile acid and lipid homeostasis. Cell 2000;102: 731–744. [PubMed: 11030617]

8). Park YJ, Kim SC, Kim J, Anakk S, Lee JM, Tseng HT, et al. Dissociation of diabetes and obesity in mice lacking orphan nuclear receptor small heterodimer partner. J Lipid Res 2011;52:2234–2244. [PubMed: 21949050]

9). Huang J, Iqbal J, Saha PK, Liu J, Chan L, Hussain MM, et al. Molecular characterization of the role of orphan receptor small heterodimer partner in development of fatty liver. Hepatology 2007;46:147–157. [PubMed: 17526026]

10). Postic C, Magnuson MA. DNA excision in liver by an albumin-Cre transgene occurs progressively with age. Genesis 2000;26:149–150. [PubMed: 10686614]

11). Wang G, Wang H, Singh S, Zhou P, Yang S, Wang Y, et al. ADAR1 prevents liver injury from inflammation and suppresses interferon production in hepatocytes. Am J Pathol 2015;185: 3224–3237. [PubMed: 26453800]

12). Holloway MG, Cui Y, Laz EV, Hosui A, Hennighausen L, Waxman DJ. Loss of sexually dimorphic liver gene expression upon hepatocyte-specific deletion of Stat5a-Stat5b locus. Endocrinology 2007;148:1977–1986. [PubMed: 17317776]

13). Kim YC, Byun S, Zhang Y, Seok S, Kemper B, Ma J, et al. Liver ChIP-seq analysis in FGF19-treated mice reveals SHP as a global transcriptional partner of SREBP-2. Genome Biol 2015;16:268. [PubMed: 26634251]

14). Lee JM, Wagner M, Xiao R, Kim KH, Feng D, Lazar MA, et al. Nutrient-sensing nuclear receptors coordinate autophagy. Nature 2014;516:112–115. [PubMed: 25383539]

15). Anakk S, Bhosale M, Schmidt VA, Johnson RL, Finegold MJ, Moore DD. Bile acids activate YAP to promote liver carcinogenesis. Cell Rep 2013;5:1060–1069. [PubMed: 24268772]

16). Tchkonia T, Morbeck DE, Von Zglinicki T, Van Deursen J, Lustgarten J, Scrable H, et al. Fat tissue, aging, and cellular senescence. Aging Cell 2010;9:667–684. [PubMed: 20701600]

17). Houtkooper RH, Argmann C, Houten SM, Canto C, Jeninga EH, Andreux PA, et al. The metabolic footprint of aging in mice. Sci Rep 2011;1:134. [PubMed: 22355651]

18). Park JH, Chung HY, Kim M, Lee JH, Jung M, Ha H. Daumone fed late in life improves survival and reduces hepatic inflammation and fibrosis in mice. Aging Cell 2014;13:709–718. [PubMed: 24796965]

19). Perry RJ, Samuel VT, Petersen KF, Shulman GI. The role of hepatic lipids in hepatic insulin resistance and type 2 diabetes. Nature 2014;510:84–91. [PubMed: 24899308]

20). Yang L, Li P, Fu S, Calay ES, Hotamisligil GS. Defective hepatic autophagy in obesity promotes ER stress and causes insulin resistance. Cell Metab 2010;11:467–478. [PubMed: 20519119]

21). Potthoff MJ, Kliewer SA, Mangelsdorf DJ. Endocrine fibroblast growth factors 15/19 and 21: from feast to famine. Genes Dev 2012;26:312–324. [PubMed: 22302876]

22). Dominguez LJ, Barbagallo M. The biology of the metabolic syndrome and aging. Curr Opin Clin Nutr Metab Care 2016;19:5–11. [PubMed: 26560521]

23). Shulman GI. Ectopic fat in insulin resistance, dyslipidemia, and cardiometabolic disease. N Engl J Med 2014;371:1131–1141. [PubMed: 25229917]

24). Kenyon CJ. The genetics of ageing. Nature 2010;464:504–512. [PubMed: 20336132]

25). Xiong X, Wang X, Lu Y, Wang E, Zhang Z, Yang J, et al. Hepatic steatosis exacerbated by endoplasmic reticulum stress-mediated downregulation of FXR in aging mice. J Hepatol 2014; 60:847–854. [PubMed: 24333182]

26). Prawitt J, Abdelkarim M, Stroeve JH, Popescu I, Duez H, Velagapudi VR, et al. Farnesoid X receptor deficiency improves glucose homeostasis in mouse models of obesity. Diabetes 2011; 60:1861–1871. [PubMed: 21593203]

27). Wang L, Liu J, Saha P, Huang J, Chan L, Spiegelman B, et al. The orphan nuclear receptor SHP regulates PGC-1alpha expression and energy production in brown adipocytes. Cell Metab 2005;2:227–238. [PubMed: 16213225]

28). Ma Y, Huang Y, Yan L, Gao M, Liu D. Synthetic FXR agonist GW4064 prevents diet-induced hepatic steatosis and insulin resistance. Pharm Res 2013;30:1447–1457. [PubMed: 23371517]

29). Watanabe M, Horai Y, Houten SM, Morimoto K, Sugizaki T, Arita E, et al. Lowering bile acid pool size with a synthetic farnesoid X receptor (FXR) agonist induces obesity and diabetes through reduced energy expenditure. J Biol Chem 2011;286: 26913–26920. [PubMed: 21632533]

30). Zadravec D, Brolinson A, Fisher RM, Cameheim C, Csikasz RI, Bertrand-Michel J, et al. Ablation of the very-long-chain fatty acid elongase ELOVL3 in mice leads to constrained lipid storage and resistance to diet-induced obesity. FASEB J 2010;24:4366–4377. [PubMed: 20605947]

31). Kobayashi T, Fujimori K. Very long-chain-fatty acids enhance adipogenesis through coregulation of Elovl3 and PPARgamma in 3T3-L1 cells. Am J Physiol Endocrinol Metab 2012;302:E1461–E1471. [PubMed: 22436697]

32). Ji L, Gupta M, Feldman BJ. Vitamin D regulates fatty acid composition in subcutaneous adipose tissue through Elovl3. Endocrinology 2016;157:91–97. [PubMed: 26488808]

33). Brolinson A, Fourcade S, Jakobsson A, Pujol A, Jacobsson A. Steroid hormones control circadian Elovl3 expression in mouse liver. Endocrinology 2008;149:3158–3166. [PubMed: 18292190]

34). Jakobsson A, Jorgensen JA, Jacobsson A. Differential regulation of fatty acid elongation enzymes in brown adipocytes implies a unique role for Elovl3 during increased fatty acid oxidation. Am J Physiol Endocrinol Metab 2005;289:E517–E526. [PubMed: 15855229]

35). Cuervo AM, Bergamini E, Brunk UT, Droge W, Ffrench M, Terman A. Autophagy and aging: the importance of maintaining “clean” cells. Autophagy 2005;1:131–140. [PubMed: 16874025]

36). Amir M, Czaja MJ. Autophagy in nonalcoholic steatohepatitis. Expert Rev Gastroenterol Hepatol 2011;5:159–166. [PubMed: 21476911]

37). Cavallini G, Donati A, Gori Z, Pollera M, Bergamini E. The protection of rat liver autophagic proteolysis from the age-related decline co-varies with the duration of anti-ageing food restriction. Exp Gerontol 2001;36:497–506. [PubMed: 11250121]

38). Zhang C, Cuervo AM. Restoration of chaperone-mediated autophagy in aging liver improves cellular maintenance and hepatic function. Nat Med 2008;14:959–965. [PubMed: 18690243]

39). Thomas C, Gioiello A, Noriega L, Strehle A, Oury J, Rizzo G, et al. TGR5-mediated bile acid sensing controls glucose homeostasis. Cell Metab 2009;10:167–177. [PubMed: 19723493]

40). Broeders EP, Nascimento EB, Havekes B, Brans B, Roumans KH, Tailleux A, et al. The bile acid chenodeoxycholic acid increases human brown adipose tissue activity. Cell Metab 2015; 22:418–426. [PubMed: 26235421]

41). Watanabe M, Houten SM, Mataki C, Christoffolete MA, Kim BW, Sato H, et al. Bile acids induce energy expenditure by promoting intracellular thyroid hormone activation. Nature 2006; 439:484–489. [PubMed: 16400329]

42). Kim KH, Lee MS. FGF21 as a stress hormone: the roles of FGF21 in stress adaptation and the treatment of metabolic diseases. Diabetes Metab J 2014;38:245–251. [PubMed: 25215270]

43). Inagaki T, Dutchak P, Zhao G, Ding X, Gautron L, Parameswara V, et al. Endocrine regulation of the fasting response by PPARalpha-mediated induction of fibroblast growth factor 21. Cell Metab 2007;5:415–425. [PubMed: 17550777]

44). Jager J, Wang F, Fang B, Lim HW, Peed LC, Steger DJ, et al. The nuclear receptor Rev-erbalpha regulates adipose tissue-specific FGF21 signaling. J Biol Chem 2016;291:10867–10875. [PubMed: 27002153]

45). Patel R, Bookout AL, Magomedova L, Owen BM, Consiglio GP, Shimizu M, et al. Glucocorticoids regulate the metabolic hormone FGF21 in a feed-forward loop. Mol Endocrinol 2015;29:213–223. [PubMed: 25495872]

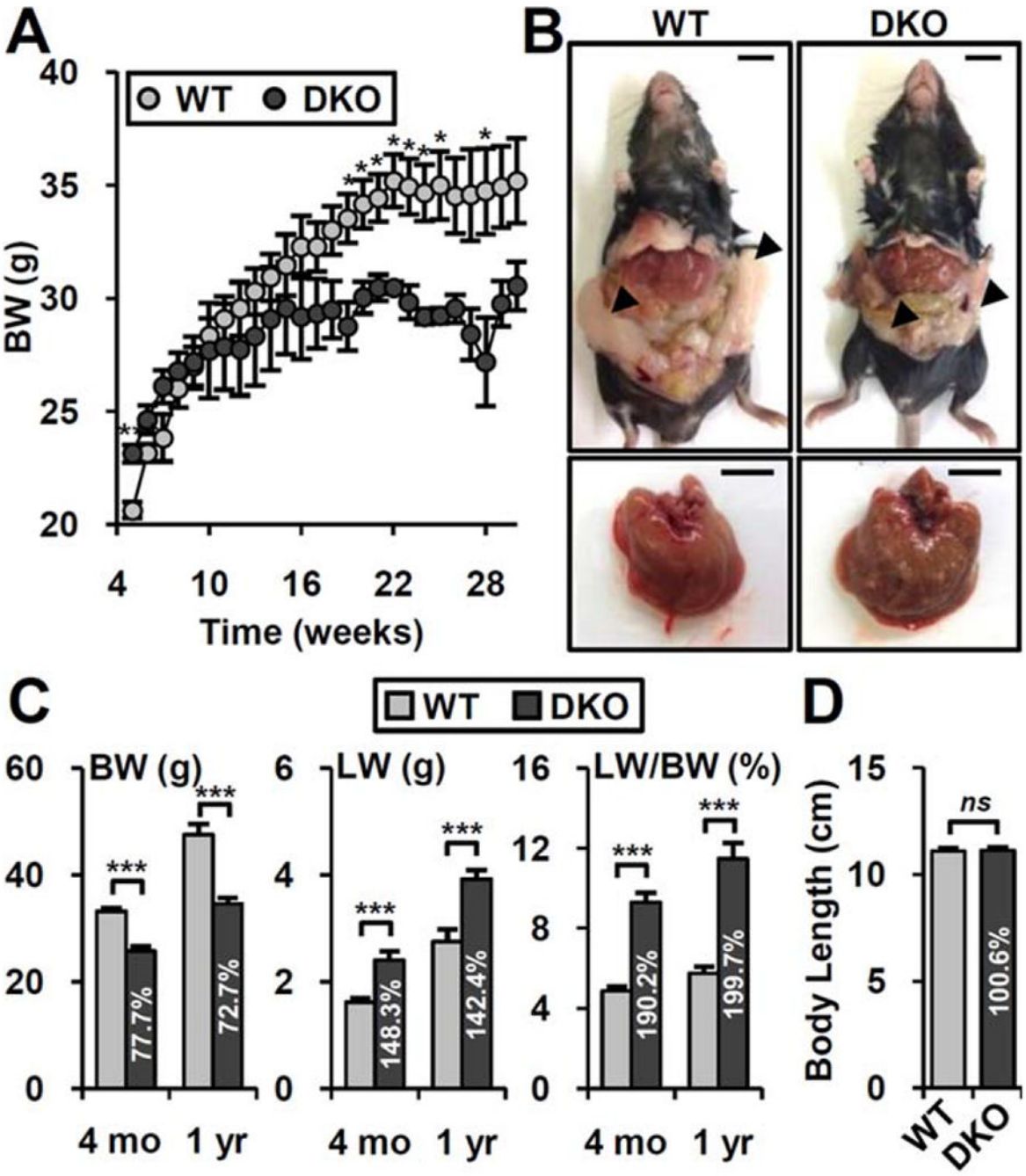

FIG. 1.

DKO mice prevent age-induced obesity. (A) Body weight changes of WT (n = 8) and DKO (n = 10) mice fed normal chow. (B) Representative picture of whole body and liver at 1 year of age. Arrowhead, epididymal adipose tissues. Scale bar, 10 mm. (C) Body weight, liver weight, and liver/body weight ratio at 4 months and 1 year of age. Values in the DKO bar graph indicated relative percentage compared to WT (percentage). (D) Body length (anal to nasal length) at 1 year of age (n = 5-8). Student *t* test: **P*< 0.05, ***P*< 0.01, ****P*< 0.005. Abbreviations: BW, body weight; LW, liver weight; ns, not significant.

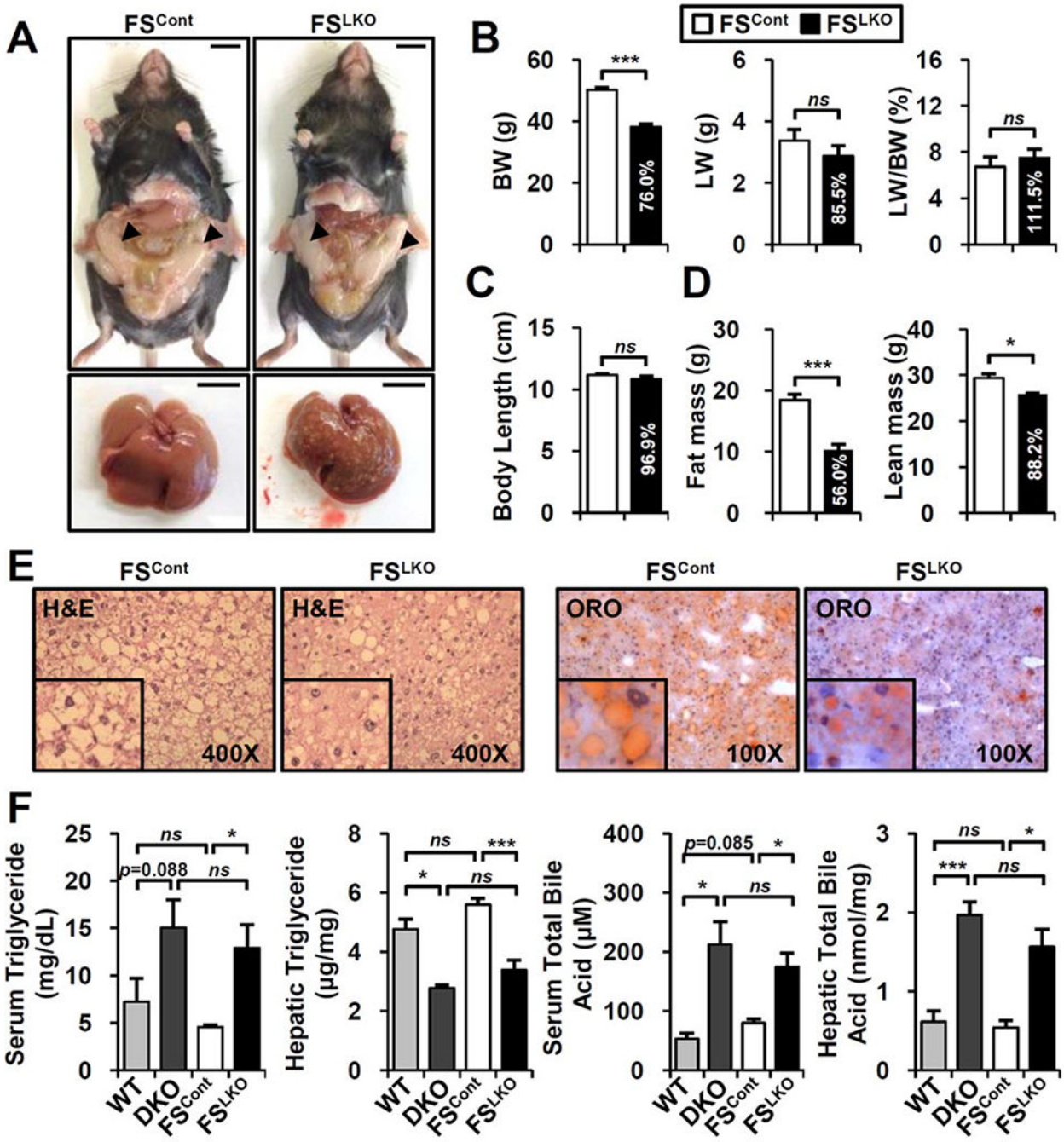

FIG. 2.

Aged FS^{LKO} mice also show a lean phenotype and have lower hepatic lipid accumulation. (A) Whole-body and liver images of normal chow-fed FS^{LKO} mice at 1 year of age. Arrowhead, epididymal adipose tissues. Scale bar, 10 mm. (B) Body weight, liver weight, and liver/body weight ratio at 1 year of age (n = 4). (C) Anal to nasal body length (n = 4). (D) Body composition of 1-year-old FS^{Cont} and FS^{LKO} mice (n = 4). (E) Hematoxylin and eosin and oil-red O staining of liver. (F) Serum and hepatic triglyceride levels and total bile acid levels in DKO and FS^{LKO} mice (n = 3-5). Student *t* test: **P*< 0.05, ****P*< 0.005.

Abbreviations: BW, body weight; H&E, hematoxylin and eosin; LW, liver weight; ns, not significant; ORO, oil-red O.

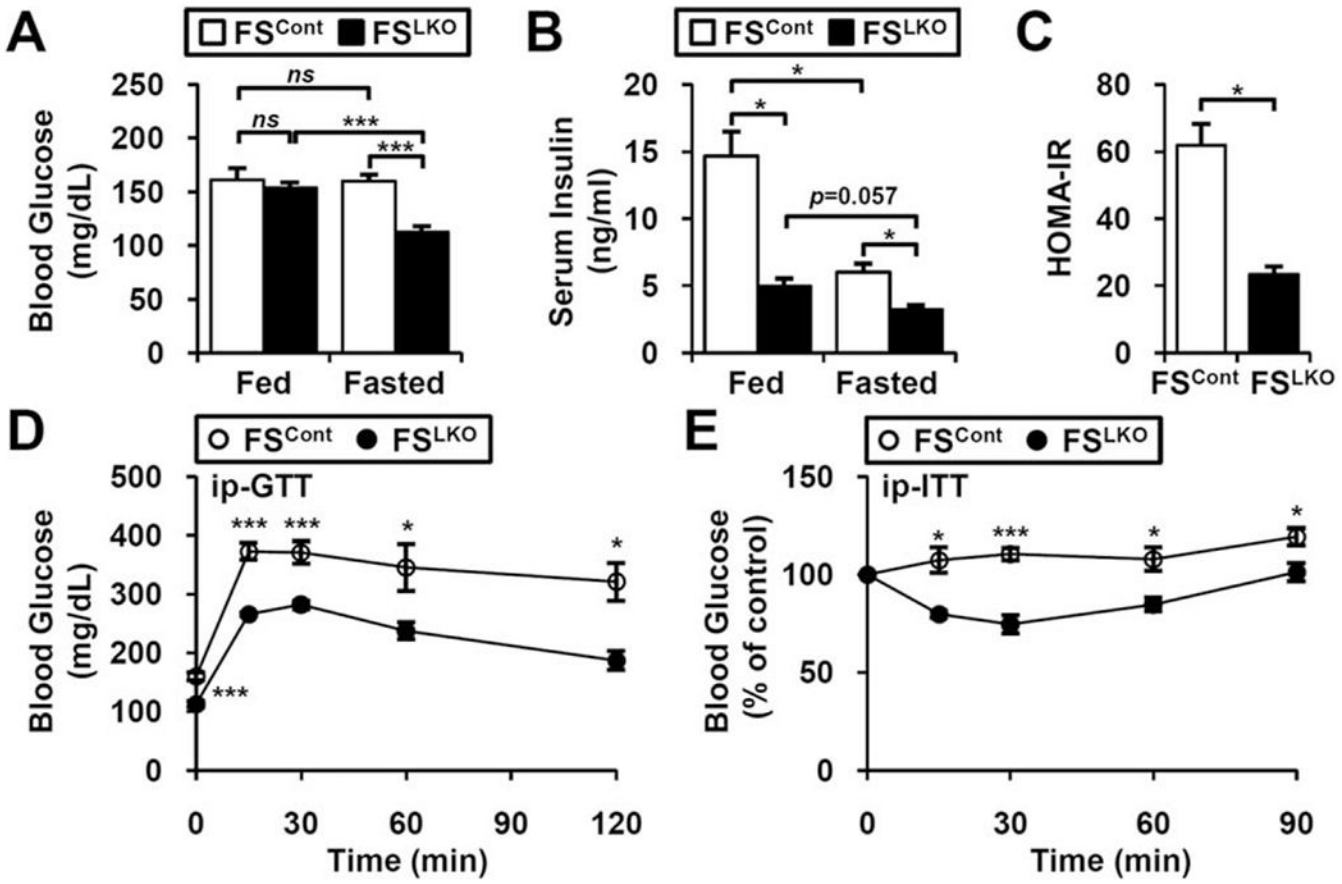

FIG. 3.

Ameliorated glucose intolerance and insulin resistance in FS^{LKO} mice. In fed and fasted conditions, (A) blood glucose and (B) serum insulin concentrations were examined at 1 year of age (n = 3-4). (C) Homeostasis model assessment of insulin resistance index of FS^{LKO} mice. (D) Glucose tolerance tests and (E) insulin tolerance tests of FS^{LKO} mice at 1 year of age (n = 4). Student *t* test: **P*< 0.05, ****p*< 0.005. Abbreviations: HOMAIR, homeostasis model assessment of insulin resistance; ip-GTT, intraperitoneal glucose tolerance test; ip-ITT, intraperitoneal insulin tolerance test; ns, not significant.

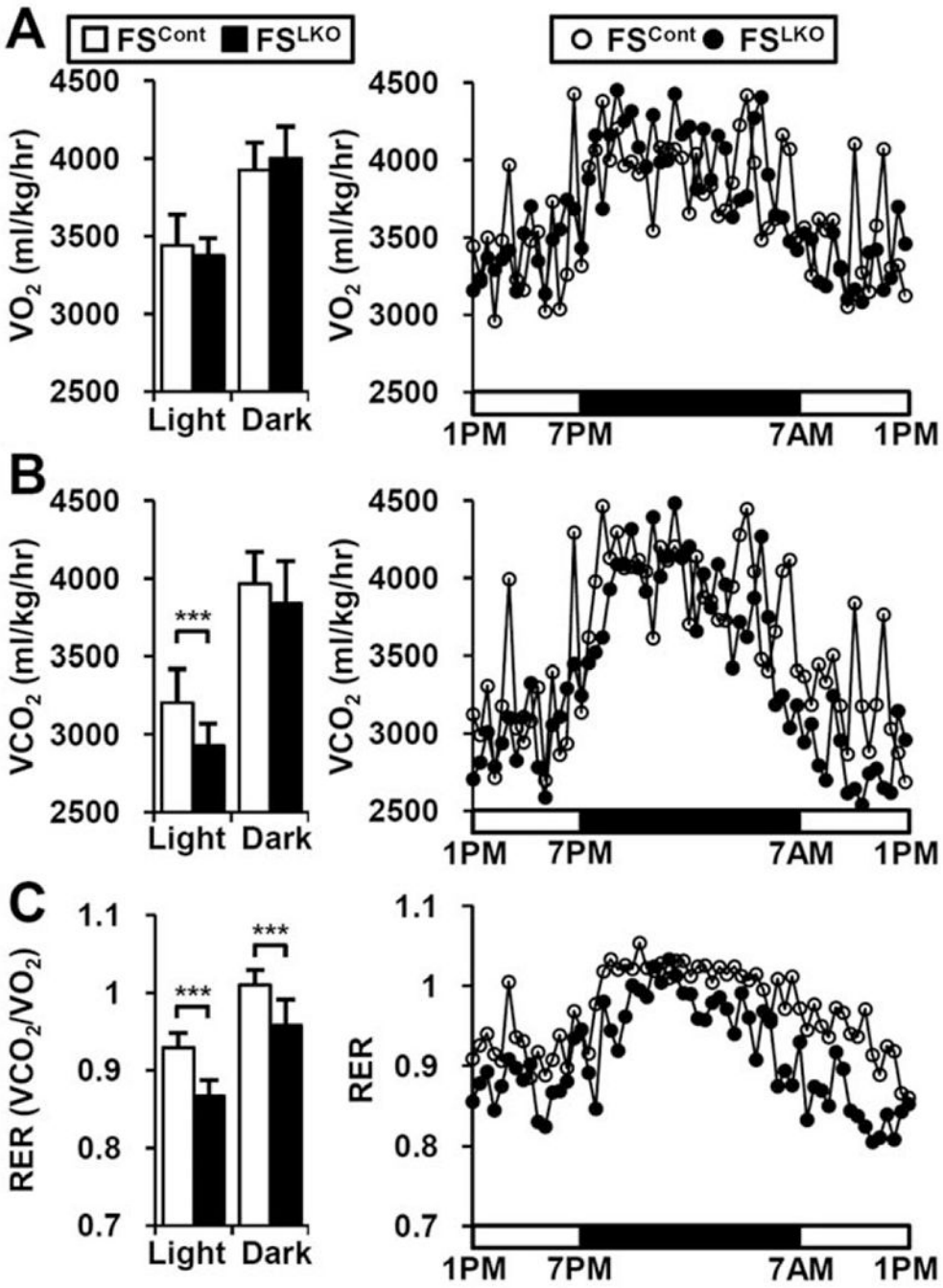

FIG. 4.

FS^{LKO} mice exhibit lower RER. Indirect calorimetry analysis of (A) oxygen consumption rate (VO_2) and (B) CO_2 production rate (VCO_2) in normal chow-fed FS^{LKO} mice (n = 3). (C) RER (VCO_2/CO_2) of FS^{LKO} mice. Data are mean of each time period ± standard error of the mean Student *t* test: ***$P < 0.005$.

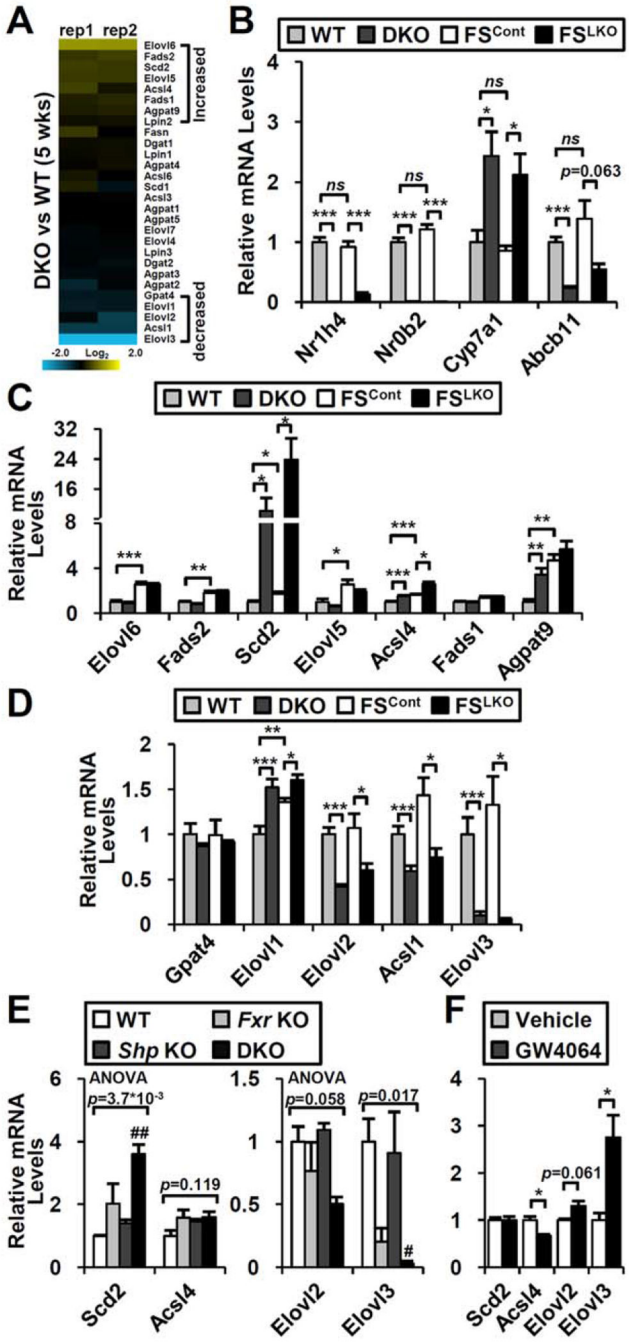

FIG. 5.

Changes of hepatic gene expression in DKO and FS^{LKO} mice. (A) Expression of fatty acid metabolism genes in DKO microarray. (B) *Fxr (Nr1h4), Shp (Nr0b2)*, and representative FXR/SHP target gene (*Cyp7a1* and *Bsep/Abcb11*) expression in 1-year-old DKO and FS^{LKO} mice (n = 4). Genes showing (C) increased or (D) decreased tendency in DKO microarray were selected, and their expression was measured in 1-year-old DKO and FS^{LKO} liver (n = 4). (E) Representative gene expression in *Fxr* and *Shp* single knockouts compared to DKO (n = 4). (F) Representative gene expression in response to FXR agonist (GW4064, 100

mg/kg) treatment (n = 4). (A-D, F) Student *t* test: **P*< 0.05, ***P*< 0.01, ****P*< 0.005. (E) One-way ANOVA, followed by *post hoc t* test: $^{\#}P$< 0.0083, $^{\#\#}P$< 0.0017 compared to WT. Abbreviation: ns, not significant.

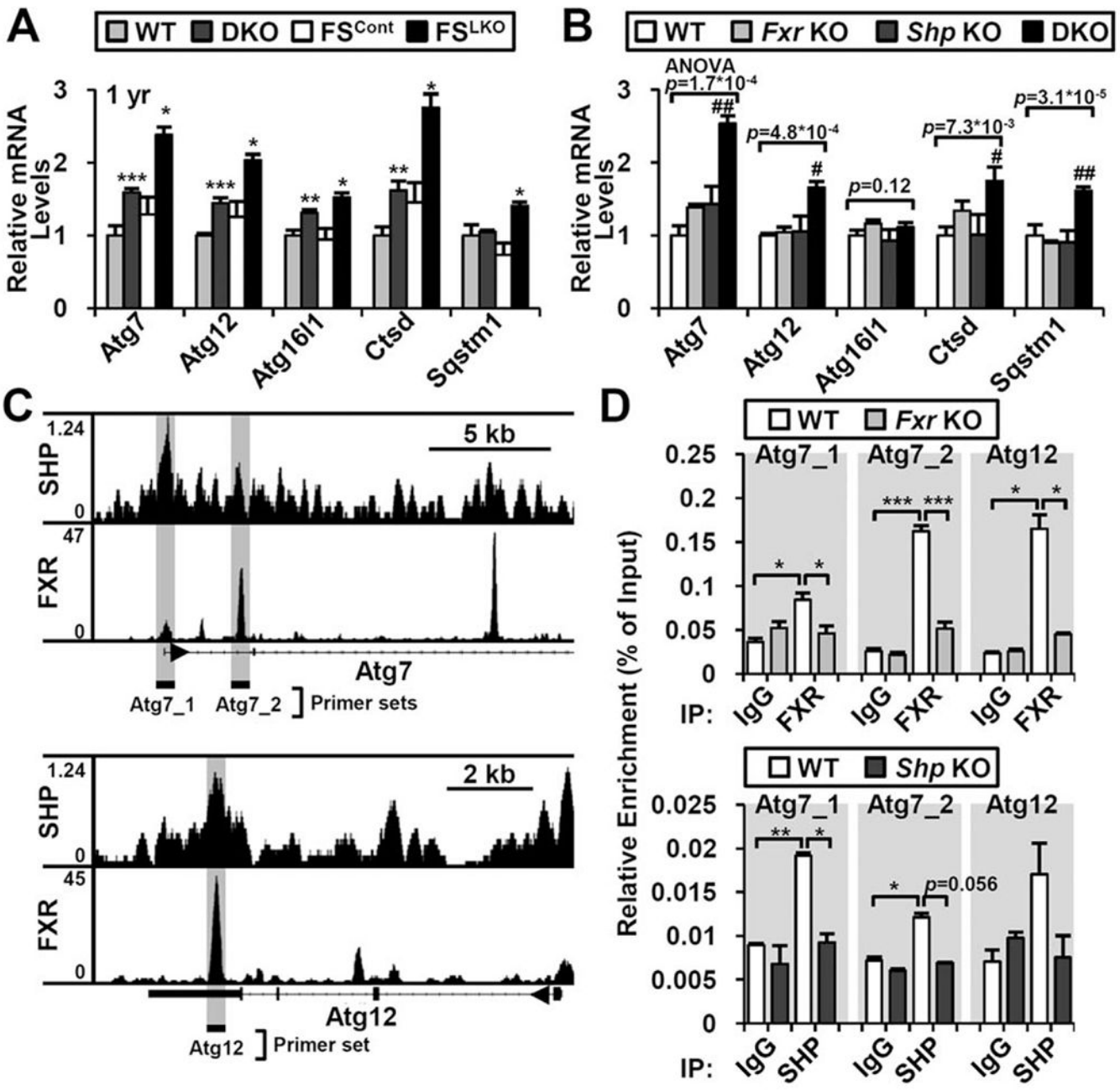

FIG. 6.

Increased autophagy-related gene expression in DKO and FS^{LKO} liver. Representative autophagy-related gene expression in (A) DKO and FS^{LKO} or (B) *Fxr* and *Shp* single knockouts (n = 3-4). (C) FXR and SHP binding at *Atg7* and *Atg12* gene loci in ChIP-seq data. Genomic loci for ChIP-PCR analysis are denoted by gray background. (D) Confirmation of FXR and SHP recruitment by ChIP-PCR analysis (n = 2-3). (A,D) Student *t* test: $^{*}P< 0.05$, $^{**}P< 0.01$, $^{***}P< 0.005$. (B) One-way ANOVA, followed by *post hoc t* test: $^{\#}P< 0.0083$, $^{\#\#}P< 0.0017$ compared to WT. Abbreviations: IgG, immunoglobulin G; IP, immunoprecipitation.

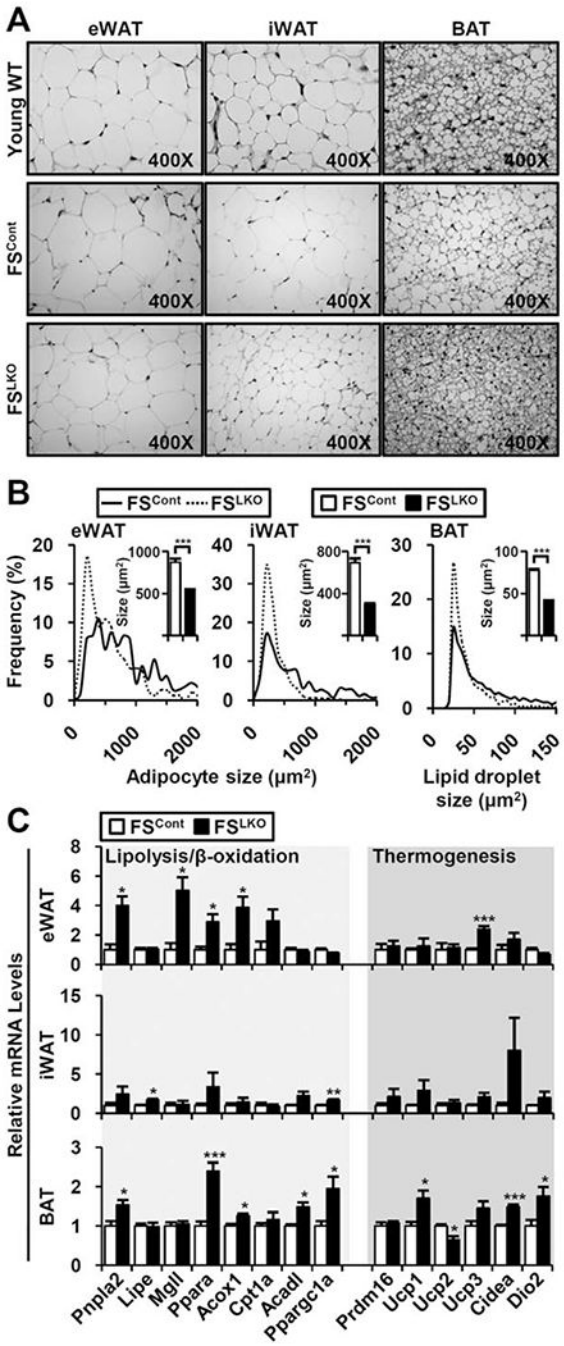

FIG. 7.

Enhanced fatty acid usage and thermogenesis gene expression in FS^{LKO} adipose tissues. (A) Hematoxylin and eosin staining of eWAT, iWAT, and BAT from young WT and old WT/DKO mice. (B) Quantification of adipocyte (eWAT and iWAT) or lipid droplet size (BAT). Inset bar graph indicates average size in square micrometers. (C) Gene expression profiles involved in lipolysis, βoxidation, and thermogenesis (n = 4). Student t test: $*P< 0.05$, $**P< 0.01$, $***P< 0.005$.